Journal of Applied Physics ARTICLE scitation.org/journal/jap

Derivation of a current-voltage-type plot beyond the Fowler-Nordheim one: The role of the voltage-dependency on the emission area

Cite as: J. Appl. Phys. **126**, 075302 (2019); doi: 10.1063/1.5116594
Submitted: 25 June 2019 · Accepted: 23 July 2019 ·
Published Online: 15 August 2019

Thiago A. de Assis[1,2,a)] and Fernando F. Dall'Agnol[3,b)]

AFFILIATIONS

[1]Institute of Physics, Federal University of Bahia, Campus Universitário da Federação, Rua Barão de Jeremoabo s/n, 40170-115 Salvador, BA, Brazil
[2]Centro Interdisciplinar em Energia e Ambiente, Federal University of Bahia, Campus Universitário da Federação, 40170-115 Salvador, BA, Brazil
[3]Department of Exact Sciences and Education (CEE), Universidade Federal de Santa Catarina, Campus Blumenau, Rua João Pessoa, 2514, Velha, Blumenau 89036-004, SC, Brazil

[a)]thiagoaa@ufba.br
[b)]fernando.dallagnol@ufsc.br

ABSTRACT

A dependency of the emission area on the applied voltage has been recently confirmed in reliable cold field emission experiments considering emitters in a large area form. In this work, we show that the inclusion of this dependency leads to a more general theory and then to a derivation of a more general current-voltage plot. This derivation is patent to a precise field emitter characterization, even in a single tip emitter form. We confirmed our analytical predictions using first-principles electrostatic calculations for a hemisphere on a cylindrical post and for ellipsoidal conducting emitters. As a consequence, a new plot is proposed beyond the Fowler-Nordheim one. This plot is experimentally feasible and provides, with high precision, the apex field enhancement factor from orthodox current-voltage characteristics.

I. INTRODUCTION

The development of methods to a precise characterization of the current-voltage characteristics (IVCs) in field emission (FE) devices, like the ones based on metal[1–3] nanostructures or carbon nanotubes (CNTs),[4–8] has been increasingly motivated to solve operating problems related to the characterization of the FE. These devices have applications as electron sources, as high-power microwave vacuum devices[9] or X-ray generators.[10–13] The commonest way to investigate an emitter is to measure IVCs (e.g., the macroscopic current, i_M, as a function of the macroscopic voltage, V_M) and extract one or more characterization parameters from an ordinary Fowler-Nordheim (FN) plot,[14] i.e., a plot of the form $\ln\{i_M/V_M^{\kappa}\}$ vs $1/V_M$, with $\kappa = 2$. Variations of the FN-plots can be considered using other variables.

An important characterization parameter in a FE device is its apex field enhancement factor (FEF). The presence of a single emitting nanoprotrusion that stands in a emitting plate of a parallel plate capacitor configuration enhances the field at its emitting apex, when subject to an applied macroscopic field, F_M. If F_M is defined in terms of the V_M by $F_M = V_M/\zeta_M$, where ζ_M corresponds to the macroscopic conversion length factor, then an apex-FEF, γ_a, is given by

$$\gamma_a = \frac{F_a}{F_M}, \tag{1}$$

where F_a corresponds to the related barrier field.

Quantifying the electrostatic field at nanometer resolution around sharp tips is of great interest for the development of FE technologies, and it is key to answer the fundamental question of how the field interacts with the sharp tips. For instance, a good agreement between the simulation and experiment has been

achieved for a sharp tungsten electron emitter with an apex radius of about 20 nm using a geometry approximated to a cone shape.[15] Careful experiments on emission from single CNTs with a radius of 7.5 nm and a length of 1.4 μm yield straight FN plots.[6] The plots concerned pass the orthodoxy test,[16] yielding experimental estimates of γ_a that are well defined constants for the CNT under analysis, i.e., depends only on the geometry of the emitter. The orthodox emission hypothesis corresponds to a set of physical and mathematical assumptions that permit a well-specified analysis of measured IVCs (see Ref. 16, p. 5). Indeed, real emission situations are never "exactly orthodox," but some real situations are expected to be nearly orthodox. In particular, the emission from a material with a good conducting path to the high-voltage supply, and emitting under high-ultra-vacuum conditions, is expected to be nearly orthodox.

A recent work[17] showed that, when the first-principles (quantum mechanical) local induced FEFs are used for CNTs, the resulting values are effectively independent of macroscopic field and behave in the same qualitative manner as the classical FEF values, corroborating the results found experimentally in Ref. 6. These results suggest that the hemisphere on a cylindrical post (HCP) model is satisfactory for the classical electrostatics of a CNT. Concentric protrusions on the emitting surface with a hemielliptical cross section has also been a useful way for modeling microgap discharge during field emission.[18] However, in these examples, the emitters are expected to have an area of emission that is dependent on the macroscopic voltage (or field). Therefore, if this dependency is not taken into account, the parameters extracted from an IVC may not be accurate. Even so, the emission is orthodox.

Comparisons between theory and experiments, in the last three decades, were primarily driven by the needs of flat panel displays and microwave amplifiers, for which the emission properties were important to know and predict, not just for the total current but also the beam spread, uniformity, and scaling with the number of tips. Such methodologies were firmly in place even before CNT's emerged as a competing field emission source. For example, the good theoretical-experimental correlation between the measured emission distribution of a single field emitter[19] would not have been possible were matters otherwise. Such a correlation required both total current and its distribution across a surface. Modeling successfully accounted for measured field forming effects.[20] This issue has also been systematically investigated in a perspective of a large area field emitter theoretically[21,22] and experimentally.[23] In Ref. 23, the authors found that for a single tungsten emitter and for several multitip emitters based on CNT and graphene, a voltage dependence in the emission area is observed. This feature suggests that a more general theory should be used to understand how this dependence influences a reliable interpretation of the IVCs, even in a single emitter form.

In this work, we develop a method than can be used to improve the quantitative interpretation of FN-plots and improve the accuracy of extracting apex-FEF values, when there is voltage dependence in emission area. This paper is organized as follows. In Sec. II, we derive and introduce a new current-voltage plot. In Sec. III, we present theoretical evidence of the linear behavior of the new plot, by electrostatic calculations, and explain the advantages of using our theory and how to extract characterization parameters. In Sec. IV, we apply the new plot to experimental data. In Sec. V, we summarize our conclusions and prospects.

II. DERIVATION OF A NEW CURRENT-VOLTAGE PLOT

We start from the connection between i_M and the characteristic current density J_C, linking experimental observations to field emission theories. We assume here that our emitters are "ideal,"and have no "complications," such as (among others) current dependence in field enhancement factors or space-charge effects. The quantity J_C is often associated with the site in the emitter with the maximum FEF, that is, in a single tip with a smooth classical surface, located at the apex. The practical use of this convention is because it mimics the historical convention by Stern-Gossling-Fowler.[24] The macroscopic emission current can be written as

$$i_M = \alpha_n A_M J_C = \alpha_f A_M J_{kC}, \tag{2}$$

where the macroscopic area A_M is the whole area or "footprint" of the emitter's plate, α_n is the notional area efficiency, and $\alpha_f \equiv \lambda_C \alpha_n$ is the formal area efficiency.[25] Values of α_n and α_f are not well known but are thought to lie in the range from 10^{-9} to 10^{-4}.[25] If α_f is constant for the range of F_M considered, then i_M is expected to be proportional to J_C in an orthodox emission.[16] The prefactor λ_C is a correction factor that takes into account various effects disregarded in conventional treatments of emission theory, such as atomic-level wave functions, for example. Neither the functional behavior nor the accurate values for λ_C are known. Currently, the best guess is that λ_C lies in the range $0.005 < \lambda_C < 14$, based on the work by Modinos[26] and, more recently, Lepetit.[2,27] In our theoretical approach, possible field dependence on λ_C is disregarded. Since our results do not depend qualitatively on what value is assumed for λ_C,[27] we assume $\lambda_C = 1$ in this work. Finally, the characteristic kernel current density J_{kC} is a mathematical quantity that can be evaluated exactly when values for the work function, ϕ, and F_a are given.

If the formal area of emission ($A_f \equiv \alpha_f A_M$) depends on F_M, then from Eq. (2), a parameter ω_0 can be defined as follows:

$$\omega_0 \equiv \frac{\partial\{\ln[i_M]\}}{\partial\{\ln[J_{kC}]\}} = 1 + \frac{\partial\{\ln[\alpha_f]\}}{\partial\{\ln[J_{kC}]\}}. \tag{3}$$

Ultimately, ω_0 gauges the variation of A_f with F_M. In our theoretical approach, possible field dependence on ω_0 is disregarded, a reasonable approximation, as we will show later. By integrating Eq. (3), a formal area efficiency, dependent on F_M, can be written as

$$\alpha_f(F_M) = \alpha_f^0 \left[\frac{J_{kC}}{J_{kC}^0}\right]^{(\omega_0 - 1)}, \tag{4}$$

where α_f^0 and J_{kC}^0 can be considered as reference values for a given turn-on macroscopic field, denoted hereafter by F_M^0. Of course, if $\omega_0 = 1$, i.e., the formal area of emission does not depend on F_M, the strictly orthodox emission hypothesis is restored as $\alpha_f(F_M) = \alpha_f^0 \Rightarrow A_f(F_M) = A_f^0$, where A_f^0 is the formal area at F_M^0.

The macroscopic emission current, from Eqs. (2) and (4), is given by

$$i_M = i_M^0 \left[\frac{J_{kC}}{J_{kC}^0}\right]^{\omega_0}, \tag{5}$$

where i_M^0 is the turn-on current of the related device.

Next, we determine J_{kC}. We use the standard FN theory, which is motivated here by the following arguments: (i) the Schottky-Nordheim (SN) barrier was well-justified when many body effects were used;[28] (ii) recent experimental findings suggesting that the analysis using the SN barrier yields emission area values much closer to each other and much closer to the electron microscopy-derived results than does analysis using the exactly triangular (ET) barrier.[29] These latter results provide a simple "experimental" confirmation that the SN barrier is a better model for real emitters than is the ET barrier. Therefore, the equations related to the SN barrier should be used to interpret $i_M - V_M$ characteristics in single tip emitters.[29] We assume that the local work function, ϕ, is constant across the surface. J_{kC} is given in terms of ϕ and the characteristic local barrier field by the equation

$$J_{kC} = a\phi^{-1}F_a^2 \exp\left[-v_F b\phi^{3/2}/F_a\right], \tag{6}$$

where a and b are first and second FN constants, respectively[16] and v_F is an appropriate particular value (relevant to the values of ϕ and F_a) of the principal SN barrier function v,[30] associated with an electron in the Fermi level moving perpendicular and toward the emitter surface.

For convenience, we use the simple approximation $v_F = 1 - f + (f/6)\ln(f)$,[30] where $f = F_a/F_R = c_s^2\phi^{-2}F_a$. Here, c_s is Schottky's constant and F_R is the reference field necessary to reduce an SN barrier from ϕ to zero.[16] Thus, J_{kC} can be written as follows:[31]

$$J_{kC} = a\phi^{-1}\exp(\eta)(F_R)^{\eta/6}(F_a)^{\kappa}\exp\left[-b\phi^{3/2}/F_a\right], \tag{7}$$

where $\kappa = 2 - \eta/6$, η being defined as $\eta \equiv bc_s^2\phi^{-1/2}$.

By using Eqs. (1) and (7), it is possible to derive the term that appear at the right-hand side of the Eq. (5) as

$$\left[\frac{J_{kC}}{J_{kC}^0}\right]^{\omega_0} = \left[\frac{F_M}{F_M^0}\right]^{\omega_0\kappa}\exp\left\{-\left[\frac{b\phi^{3/2}\omega_0}{\gamma_a}\right]\left[\frac{1}{F_M} - \frac{1}{F_M^0}\right]\right\}. \tag{8}$$

Finally, replacing Eq. (8) in Eq. (5), we can write

$$\ln\left\{C(F_M^0, i_M^0) \times \frac{i_M}{(F_M)^{\kappa\omega_0}}\right\} = -\frac{b\phi^{3/2}\omega_0}{\gamma_a}\left[\frac{1}{F_M} - \frac{1}{F_M^0}\right], \tag{9}$$

where $C(F_M^0, i_M^0) \equiv (F_M^0)^{\kappa\omega_0}/i_M^0$. All quantities ω_0, F_M^0, i_M^0, $C(F_M^0, i_M^0)$, and κ can be, in principle, obtained experimentally. Even if experimental conditions are similar to our theory, extract ω_0 requires the knowledge of the local current density at the apex. Until recently, the best attempt to reliably measure the current density was the work by Dyke and colleagues.[32] Recently, experimental studies on glow pattern analysis were conducted over a wide range of emission currents and were able to estimate a characteristic local current density in large area carbon-based emitters in a polymer matrix.[33]

III. ROLE OF THE NEW CURRENT-VOLTAGE PLOT: ELECTROSTATIC CALCULATIONS AND EXTRACTION OF CHARACTERIZATION PARAMETERS

Now, we show the role of the plot proposed by Eq. (9) in extracting γ_a. We simulate the FE from HCP[34–40] and ellipsoidal[41] emitters. In order to solve the Laplace equation to calculate the local electrostatic field distribution, we have used the commercial software COMSOL v5.3a based on the finite elements method to calculate the local electrostatic field at the emitter's surface and then the macroscopic current. Details of the simulation procedure to find γ_a numerically, follow the same lines as reported in Ref. 42.

Simulations that involve the solution of Laplace's equation, whether using finite elements or finite differences, require a minimum volume surrounding the region of interest. The minimum domain size depends on the desired precision. If the boundaries are inadvertently close, they will affect the calculated electrostatic potential and the FEF may not respect the desired precision. Then, it might be attempting to overestimate the size of the domain. However, this procedure may become seriously time and memory consuming, as the simulated systems become more demanding, mainly in three dimensional and/or in time-dependent models. We employed the minimum domain size analysis in Ref. 42 to determine the best size of our simulation domain.

Our analyses considers a two dimensional (2D) axisymmetric system. Figure 1 represents the geometries of the physical systems. It is a 2D axisymmetric system with a central emitter. We assume the emitter to be a perfect conductor with no electric field penetration; hence, the interior of the emitter is removed from the simulation domain. The boundary conditions (BCs) on the emitter's surface and the bottom surface are grounded ($\Phi = 0$ V). The right-hand side boundary is a symmetry line, i.e., this BC imposes the electrostatic field to be perpendicular to the normal vector from this boundary line ($\mathbf{F}\cdot\hat{\mathbf{n}} = 0$). The top boundary is set as a surface charge density $\sigma = \epsilon_0 F_M$, where ϵ_0 is the permittivity of vacuum. This BC assumes that the anode is much farther than the boundary itself.

The apex-FEF numerically calculated, γ_a, is defined as the maximum value of the electrostatic field normalized by the macroscopic field. The finite elements were concentrated where the electric field was higher and the number of elements was increased until the solution converged to the necessary precision for our purposes.

Experimentally, the range of i_M is what determines the range in F_M, i.e., F_M varies until the emission curve is obtained from turn-on up to maximum current obtainable without burning the emitter. In our electrostatic simulations, we consider $i_M = \int_{cap} J_\ell dA$ integrated over the cap of the emitter, with J_ℓ being the local current density on the emitter's surface, given by Eq. (6), replacing the index kC by ℓ and F_a by F_ℓ. The emitter's surface and the

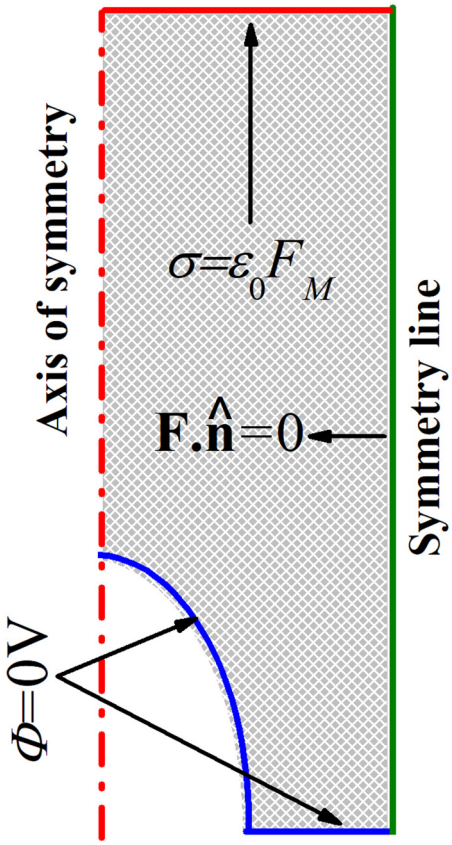

FIG. 1. Representation of the physical system and the boundary conditions to simulate field emission. The top boundary is a Neumann boundary condition that imposes a vertically aligned electrostatic field as if the anode were much farther.

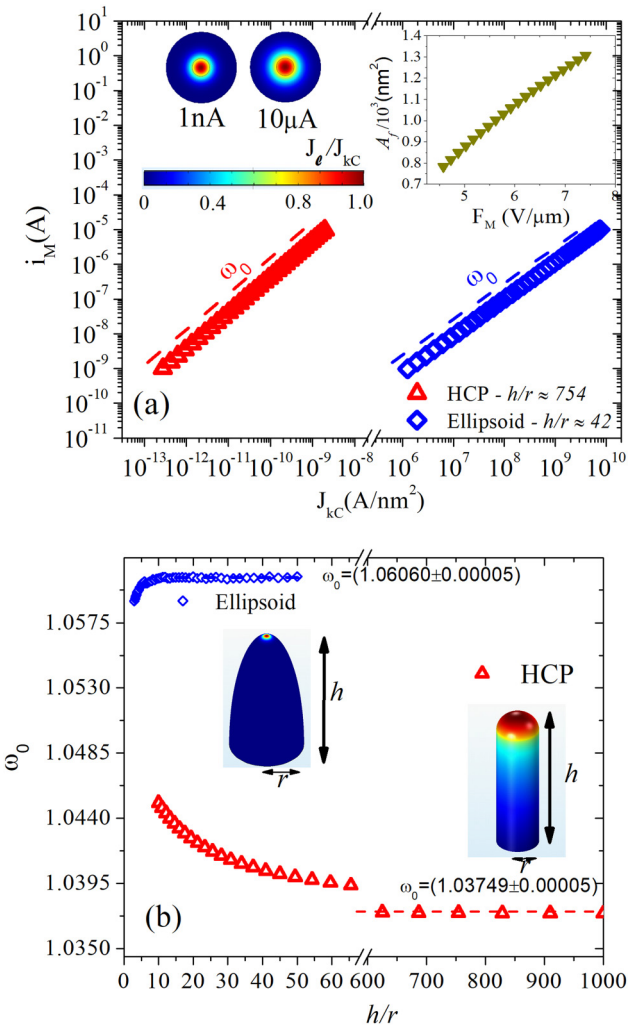

FIG. 2. (a) Macroscopic current as a function of the characteristic kernel current density, in log-log scale, for HCP ($h/r \approx 754$) and ellipsoidal ($h/r \approx 42$) emitters. The dashed lines correspond to linear fits in order to calculate ω_0, according to Eq. (5). The insets at the top are as follows: (left) top view of ellipsoidal emitters with $h/r = 50$, $i_M = 1$nA and $i_M = 10\,\mu$A. The color map displays the local ratio $0 \leqslant J_\ell/J_{kC} \leqslant 1$, where J_ℓ is the local current density; (right) formal area, A_f, calculated using Eq. (4), as a function of F_M for a ellipsoidal emitter with $h/r = 50$. (b) ω_0-values as a function of the aspect ratio, for HCP and ellipsoidal emitters. Notice the saturation of the ω_0-values in the limit of high aspect ratios (horizontal dashed lines). The estimation of the ω_0-values in this limit is also shown for both emitters.

substrate are grounded ($\Phi = 0$ V). The interior of the emitter has no electric field and can be excluded from the simulation domain. The apex-radii of curvature for both emitters are 50 nm in all simulations. Figure 2(a) shows the macroscopic current as a function of the characteristic kernel current density, for HCP and ellipsoidal emitters with aspect ratio $h/r \approx 754$ and $h/r \approx 42$, respectively. These plots enable us to calculate ω_0 from a linear fit confirming that $i_M \sim (J_{kC})^{\omega_0}$, as predicted in Eq. (5). The inset shows the top view of an ellipsoidal emitter with $h/r = 50$, $i_M = 1$ nA or $i_M = 1\,\mu$A. The color map shows the J_ℓ/J_{kC} distribution. Note that the distribution is more spread at high currents, implying a larger area of emission. This is clear justified since the formal area A_f for a ellipsoidal emitter with $h/r = 50$, evaluated by using Eq. (4), has been found to increase with F_M, as shown in the inset of Fig. 2(a). This result quantitatively corroborates with Fig. 2(b), in which ω_0-values are larger than unity. Interestingly, ω_0 saturates in the limit of high aspect ratios that is preferred in most technological applications. Note that ω_0 is larger for ellipsoidal emitters, showing that the change of the formal area of emission with F_M is larger in this case. This result confirms other reports using different shapes.[43] Also, analytic forms of the area factor change depending on how the field falls off over the surface.[44,45] Indeed, we found $\omega_0 = (1.037\,49 \pm 0.000\,05)$ for HCP emitters with $h/r \gtrsim 600$ and $\omega_0 = (1.060\,60 \pm 0.000\,05)$ for ellipsoidal emitters with $h/r \gtrsim 15$.

Figure 3 shows the results for the FN-type plots. These plots are linear under the transformation of coordinates done in Eq. (9),

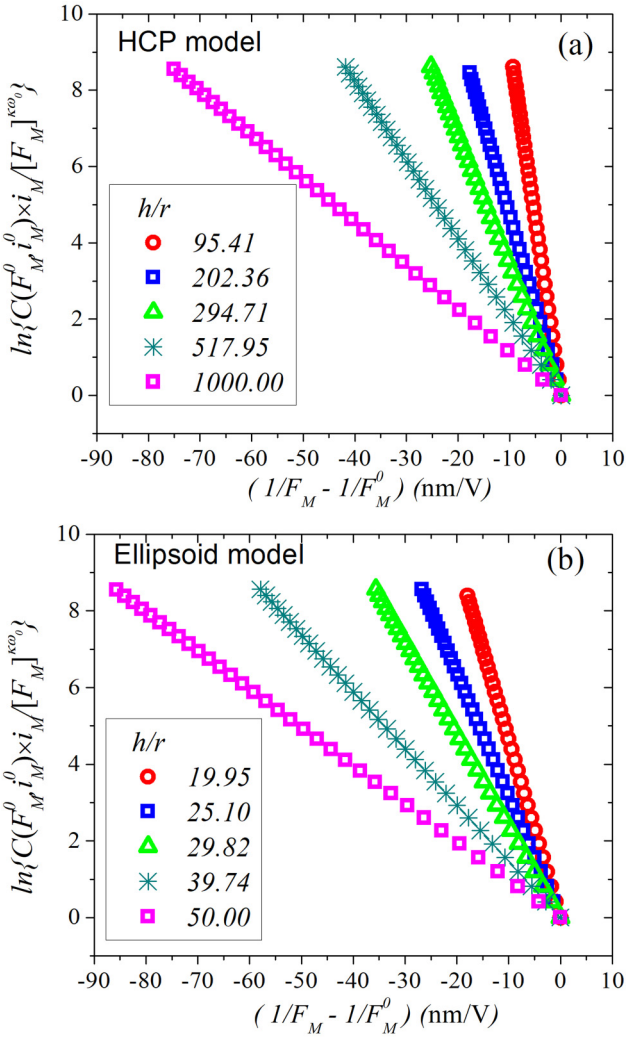

FIG. 3. Plots, as proposed in Eq. (9), for (a) HCP and (b) ellipsoidal emitters, for various aspect ratios. ω_0-values were extracted from the results shown in Fig. 2.

which is consistent with the dependence of the A_f on F_M. Also, for each emitter, absolute values of the slopes decreases when h/r increases. These features suggest that an apex-FEF, γ_{exp}, can be extracted experimentally as follows:

$$\gamma_{exp} = -\frac{\omega_0 b \phi^{3/2}}{S_{fit}}, \tag{10}$$

where S_{fit} denotes the slope of the straight line fitted to a FN-type plot of the $i_M \times F_M$ data. A relevant issue should be discussed at this point. Consider a traditional FN-plot $\ln\{i_M/F_M^{\kappa}\}$ vs $1/F_M$, with $\kappa = 2$. Will the experimental conditions pass the orthodox test, even if the formal area of emission depends on F_M? Let us check if our data passes the orthodox test although the formal area of emission is voltage-dependent. In order to investigate this, let us consider the corresponding scaled barrier parameter extracted from our theoretical FN-plots (not shown), which is $f_{ext} = -s_t\eta/[S_{fit}(1/F_M)_{ext}]$.[16] Here, $(1/F_M)_{ext}$ is the experimental value read from the horizontal axis of the FN-plot. In this work, we assumed $(1/F_M)_{ext}$ to be near the midpoint of the range of $1/F_M$. Additionally, a good approximation, considering SN barrier, is $s_t \approx 0.95$.[16] Although the data presented in Figs. 4(a) and 4(b) are consistent with the orthodoxy hypothesis, the formal area of emission is sensibly voltage-dependent ($\gtrsim$ 80%; see Fig. 2). These data were obtained for work function $\phi = 4.5$ eV. In addition, the barrier field extracted, f_{ext}, was considering the whole data range, lying between f_{low} and f_{up} boundaries. Indeed, an improved test, introduced in Ref. 46, extracts f-values including the whole range of experimental data. For an FN-plot of $i_M(F_M)$ for an SN barrier, the f-values relating to the macroscopic field F_M at lower and upper range in an FN-plot is given theoretically by

$$f_{low,up} = -\frac{s_t\eta}{S_{fit}(1/F_M)_{low,up}}, \tag{11}$$

where $(1/F_M)_{low,up}$ is the experimental value read from the horizontal axis of the FN-plot at lower and upper end of the range in an FN-plot considered. Our results suggest that, for all emitters considered here, the dependence of α_f on F_M [see Eq. (4)] is not large enough to fail the orthodoxy test. Then, it is possible to extract, from an ordinary FN-plot, the FEF γ_{FNplot}. This quantity, which is often used by experimentalists to estimate a apex-FEF, is given by

$$\gamma_{FNplot} = -\frac{s_t b \phi^{3/2}}{S_{FNplot}}, \tag{12}$$

where S_{FNplot} is the slope of the ordinary FN-plot, calculated by applying linear regression to the data points. In order to prove the advantage of the plot given by Eq. (9), let us define an error $\varepsilon \equiv (\gamma - \gamma_a)/\gamma_a \times 100(\%)$, where γ is given by Eq. (10) or (12). γ_a is given by Eq. (1) and was obtained from first-principles electrostatic calculations.[42] Figure 4(c) shows ε as a function of h/r from the two emitters considered here and the two plots, namely, that proposed by Eq. (10) and the ordinary FN-plot. The errors considering an ordinary FN-plot are between 4.5% and 7%. For the plot given by Eq. (10), the agreement is three orders of magnitude lower. Actually, the agreement is exact considering the systematic error due to the finite size of the simulation domain.[42] These results firmly show that the inclusion of the formal area dependency on macroscopic voltage leads to a more general theory beyond that from the FN-plots or even the Murphy-Good plot[47] to a precise field emitter characterization, even in a single tip emitter form, corroborating the arguments reported in Refs. 48 and 49. We emphasized that such dependencies in the area are explicitly required if one is modeling a field emitter similarly to the ones as presented here. We stress that field dependent emission areas were already implicit in analytical or numerical integration of current

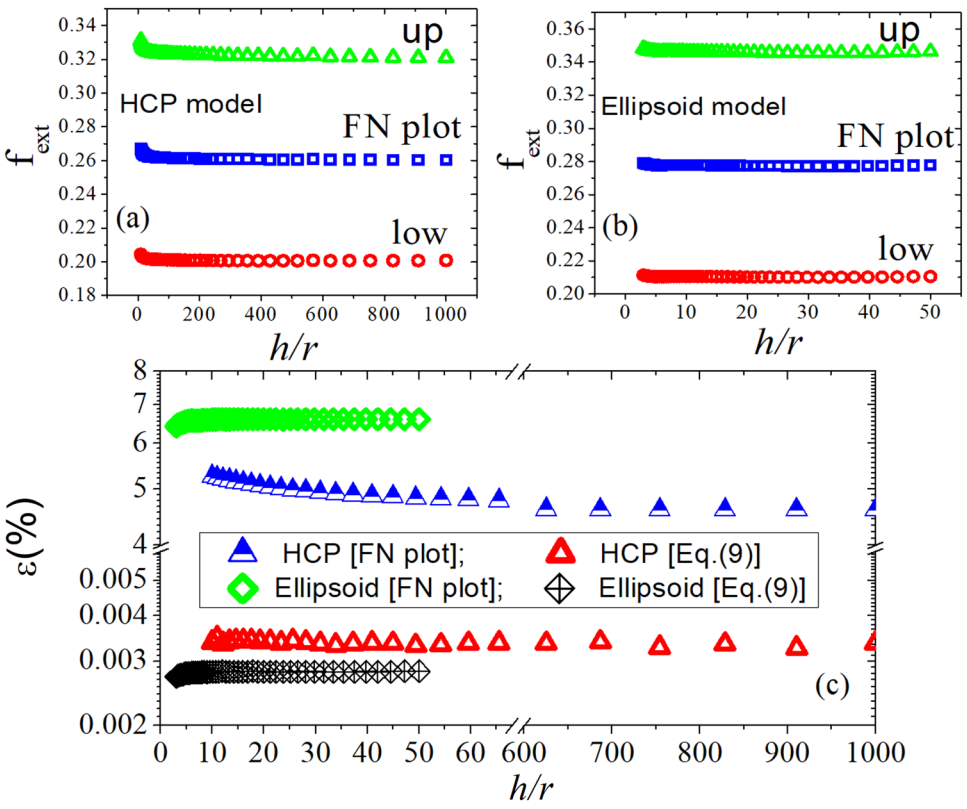

FIG. 4. Extracted scaled barrier fields from FN-plots, f_{ext}, f_{up}, and f_{low} [see Ref. 46 for details] as a function of h/r, for (a) HCP and (b) ellipsoidal emitters. (c) Errors on the extraction of the apex-FEF from a FN-plot and the plot proposed in Eq. (9) as a function of h/r.

density over a surface to find total current in single emitter (or as one of many).[44,49–55]

IV. APPLYING AND CONFIRMING THE NEW PLOT TO EXPERIMENTAL DATA

Finally, we confirm a good linear behavior of our plot considering experimental data for a tungsten emitter (X89),[32] where current-voltage measurements are available. For a tungsten emitter (X89),[32] there are current-voltage measurements available. A reanalysis of this IVCs data, using our improved plot [see Eq. (9)], yields results shown in Fig. 5. In order to make the plot, we considered the variable F_M instead of measured voltage (V_m), as used in Ref. 32. To make this conversion, we considered the distance emitter plate to anode plate $d_{sep} = 0.5$ cm, the same as reported in Ref. 32. We point out that using F_M as independent variable, instead of "macroscopic" voltage, is convenient since metal systems, as those used in Ref. 32, are usually ideal. However, we chose plots against $1/V_m$ to be more practice because V_m is measured directly, whereas F_M is not.[56] We consider also that the emitter has the form of a semiellipsoid with similar geometry as shown in Fig. 7 of the Ref. 32. Then, $\omega_0 \approx 1.060\,60$. Finally, the work function is $\phi = 4.5$ eV, which produces $\kappa = 2 - \eta/6 = 1.2272$.

These results provide confirmation that our new plots produce good straight lines, making possible to extract improved characterization parameters. From Eq. (10), we obtained an extracted FEF of about 6721. Also, the extracted field to voltage conversion factor (β) was estimated as $\beta \approx 1.34 \times 10^4\ \mathrm{cm}^{-1}$, which is a little bit larger as compared with the value $\beta = (9.9 \pm 1.5) \times 10^3\ \mathrm{cm}^{-1}$ found in Ref. 32. This tendency is the same, as observed theoretically in the paper, when we compare the characterization

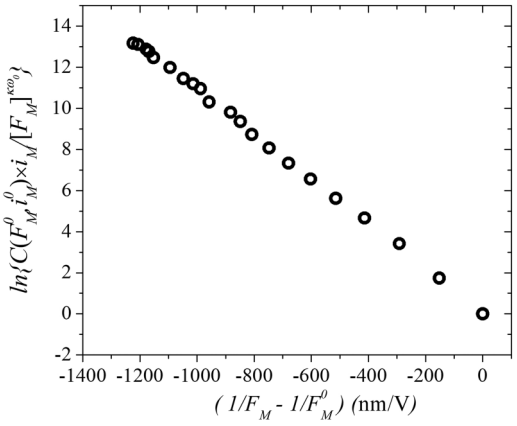

FIG. 5. Plots, as proposed in Eq. (9), considering the IVCs data from a tungsten emitter (X89), as shown in Fig. 3 of Ref. 32.

parameters extracted from an ordinary FN-plot and that we proposed in Eq. (9).

V. CONCLUSIONS

Possibilities to apply our results in nanoscale include a recent work based on the analysis of a three dimensional numerical quantum mechanical model of electronic field emission from metallic surfaces with nanoscale corrugation.[3] In this work, local and emitted current densities were obtained by using the time-dependent perturbation theory. Thus, it would be interesting to compare the FEF extracted from Eq. (10) and the one defined from the first-principles.[1,17] Also, a recent research study has determined the local electrostatic field at a nanoemitter under field emission conditions by differential phase contrast in scanning transmission electron microscopy, assuming cylindrical symmetry.[15] If current-voltage characteristics are possible to be measured, then it will be possible to verify the differences between the FEFs extracted from them and the ones found by experimental measurements of the local electrostatic field at the emitter's apex.

The theory described in this work has potential to improve the characterization of emitters in a large area form. If multiple emitters are involved, then one takes into account the local field distribution over the emitters.[53,57] All this upsets how the Fowler-Nordheim theory is commonly (and incorrectly) applied. As a recent example, an excellent agreement between experimental characteristics from CNT-based emitters and a two-class FEF model theory was confirmed.[58] Also, a nearly power-law dependence between i_M and J_{kC} was experimentally confirmed.[59] The authors of this work urge for experimental tests with CNT-based large area emitters, considering ω_0 extracted from a $i_M - J_{kC}$ plot, similar to that presented in Fig. 2, which is feasible by using a brightness level technique observed in glow pattern analyses.[59,60]

ACKNOWLEDGMENTS

The authors thank CNPq (Brazilian agency) and Dr. Richard G. Forbes for discussions and for providing the experimental current-voltage characteristics for a tungsten emitter (X89) from Dyke and Trolan's paper.[32]

REFERENCES

[1]B. Lepetit, D. Lemoine, and M. Márquez-Mijares, J. Appl. Phys. **120**, 085105 (2016).
[2]B. Lepetit, J. Appl. Phys. **122**, 215105 (2017).
[3]B. Lepetit, J. Appl. Phys. **125**, 025107 (2019).
[4]J. Robertson, Mater. Sci. Eng. R Rep. **37**, 129 (2002).
[5]J.-M. Bonard, H. Kind, T. Stöckli, and L.-O. Nilsson, Solid State Electron. **45**, 893 (2001).
[6]J.-M. Bonard, K. A. Dean, B. F. Coll, and C. Klinke, Phys. Rev. Lett. **89**, 197602 (2002).
[7]M. T. Cole, M. Mann, K. B. Teo, and W. I. Milne, in *Emerging Nanotechnologies for Manufacturing, Micro and Nano Technologies*, 2nd ed., edited by W. Ahmed and M. J. Jackson (William Andrew Publishing, Boston, 2015), pp. 125–186.
[8]E. Marcelino, T. A. de Assis, C. M. de Castilho, and R. F. Andrade, Phys. Rev. Appl. **11**, 014012 (2019).
[9]D. R. Whaley, B. M. Gannon, C. R. Smith, C. M. Armstrong, and C. A. Spindt, IEEE Trans. Plasma Sci. **28**, 727 (2000).
[10]M. T. Cole, R. J. Parmee, and W. I. Milne, Nanotechnology **27**, 082501 (2016).
[11]E. Gidcumb, B. Gao, J. Shan, C. Inscoe, J. Lu, and O. Zhou, Nanotechnology **25**, 245704 (2014).
[12]A. Basu, M. E. Swanwick, A. A. Fomani, and L. F. Velásquez-García, J. Phys. D Appl. Phys. **48**, 225501 (2015).
[13]N. A. Moody, K. L. Jensen, A. Shabaev, S. G. Lambrakos, J. Smedley, D. Finkenstadt, J. M. Pietryga, P. M. Anisimov, V. Pavlenko, E. R. Batista, J. W. Lewellen, F. Liu, G. Gupta, A. Mohite, H. Yamaguchi, M. A. Hoffbauer, and I. Robel, Phys. Rev. Appl. **10**, 047002 (2018).
[14]R. G. Forbes, J. H. B. Deane, A. Fischer, and M. S. Mousa, Jordan. J. Phys. **8**, 125 (2015).
[15]M. Wu, A. Tafel, P. Hommelhoff, and E. Spiecker, Appl. Phys. Lett. **114**, 013101 (2019).
[16]R. G. Forbes, Proc. R. Soc. Lond. A Math. Phys. Eng. Sci. **469**, 20130271 (2013).
[17]C. P. de Castro, T. A. de Assis, R. Rivelino, F. de B. Mota, C. M. C. de Castilho, and R. G. Forbes, J. Phys. Chem. C **123**, 5144 (2019).
[18]Y. Fu, P. Zhang, J. Krek, and J. P. Verboncoeur, Appl. Phys. Lett. **114**, 014102 (2019).
[19]K. Jensen, P. Mukhopadhyay-Phillips, E. Zaidman, K. Nguyen, M. Kodis, L. Malsawma, and C. Hor, Appl. Surf. Sci. **111**, 204 (1997).
[20]P. R. Schwoebel, C. A. Spindt, and C. E. Holland, J. Vac. Sci. Technol. B **21**, 433 (2003).
[21]T. A. de Assis, Sci. Rep. **5**, 10175 (2015).
[22]T. A. de Assis, J. Vac. Sci. Technol. B **33**, 052201 (2015).
[23]E. O. Popov, S. V. Filippov, A. G. Kolosko, P. A. Romanov, and R. G. Forbes, in *2016 29th International Vacuum Nanoelectronics Conference (IVNC)* (IEEE, 2016), pp. 177–178.
[24]T. E. Stern, B. S. Gossling, and R. H. Fowler, Proc. R. Soc. Lond. A Math. Phys. Eng. Sci. **124**, 699 (1929).
[25]R. G. Forbes, Nanotechnology **23**, 095706 (2012).
[26]A. Modinos, Solid State Electron. **45**, 809 (2001).
[27]R. G. Forbes, in *31st International Vacuum Nanoelectronics Conference (IVNC)* (IEEE, 2018), pp. 126–127.
[28]N. D. Lang and W. Kohn, Phys. Rev. B **3**, 1215 (1971).
[29]R. G. Forbes, in *2015 28th International Vacuum Nanoelectronics Conference (IVNC)* (IEEE, 2015), pp. 70–71.
[30]R. G. Forbes, Appl. Phys. Lett. **89**, 113122 (2006).
[31]R. G. Forbes, Appl. Phys. Lett. **92**, 193105 (2008).
[32]W. P. Dyke and J. K. Trolan, Phys. Rev. **89**, 799 (1953).
[33]E. O. Popov, A. G. Kolosko, S. V. Filippov, and E. I. Terukov, J. Vac. Sci. Technol. B **36**, 02C106 (2018).
[34]C. J. Edgcombe and U. Valdrè, J. Microsc. **203**, 188 (2001).
[35]R. G. Forbes, C. Edgcombe, and U. Valdrè, Ultramicroscopy **95**, 57 (2003).
[36]G. C. Kokkorakis, A. Modinos, and J. P. Xanthakis, J. Appl. Phys. **91**, 4580 (2002).
[37]F. Read and N. Bowring, Nucl. Instrum. Methods Phys. Res. A **519**, 305 (2004).
[38]W. Zeng, G. Fang, N. Liu, L. Yuan, X. Yang, S. Guo, D. Wang, Z. Liu, and X. Zhao, Diam. Relat. Mater. **18**, 1381 (2009).
[39]F. F. Dall'Agnol and D. den Engelsen, Nanosci. Nanotechnol. Lett. **5**, 329 (2013).
[40]D. Roveri, G. Sant'Anna, H. Bertan, J. Mologni, M. Alves, and E. Braga, Ultramicroscopy **160**, 247 (2016).
[41]A. Kyritsakis, G. C. Kokkorakis, J. P. Xanthakis, T. L. Kirk, and D. Pescia, Appl. Phys. Lett. **97**, 023104 (2010).
[42]T. A. de Assis and F. F. Dall'Agnol, J. Vac. Sci. Technol. B **37**, 022902 (2019).
[43]H. G. Kosmahl, IEEE. Trans. Electron. Devices **38**, 1534 (1991).
[44]D. Biswas and R. Ramachandran, J. Vac. Sci. Technol. B **37**, 021801 (2019).
[45]K. L. Jensen, *Wiley Encyclopedia of Electrical and Electronics Engineering* (John Wiley & Sons, Inc., New York, 2014).
[46]R. G. Forbes, Nanotechnology **23**, 288001 (2012).
[47]R. G. Forbes, e-print arXiv:1905.07585 (2019).
[48]D. Nicolaescu, J. Vac. Sci. Technol. B **11**, 392 (1993).

[49]K. L. Jensen, D. A. Shiffler, J. J. Petillo, Z. Pan, and J. W. Luginsland, Phys. Rev. ST Accel. Beams **17**, 043402 (2014).
[50]D. A. Kirkpatrick, A. Mankofsky, and K. T. Tsang, Appl. Phys. Lett. **60**, 2065 (1992).
[51]R. L. Hartman, W. A. Mackie, and P. R. Davis, J. Vac. Sci. Technol. B **12**, 754 (1994).
[52]J. D. Zuber, K. L. Jensen, and T. E. Sullivan, J. Appl. Phys. **91**, 9379 (2002).
[53]K. L. Jensen and C. M. Marrese-Reading, J. Vac. Sci. Technol. B **21**, 412 (2003).
[54]A. G. Kusne and D. N. Lambeth, IEEE. Trans. Electron Devices **57**, 712 (2010).
[55]D. Biswas, Phys. Plasmas **25**, 043105 (2018).
[56]R. G. Forbes, private communication (2019).
[57]S. A. Guerrera, L. F. Velasquez-Garcia, and A. I. Akinwande, IEEE Trans. Electron Devices **59**, 2524 (2012).
[58]E. O. Popov, A. G. Kolosko, S. V. Filippov, and T. A. de Assis, "Influence of the distribution of local field enhancement factors on the shape of the current-voltage characteristics of carbon-nanotube-based large-area emitters," J. Appl. Phys. (submitted).
[59]E. O. Popov, S. V. Filippov, A. G. Kolosko, and T. A. de Assis, J. Appl. Phys. **126**, 044304 (2019).
[60]E. O. Popov, A. G. Kolosko, S. V. Filippov, and E. I. Terukov, J. Vac. Sci. Technol. B **36**, 02C106 (2018).